Response of modern fluvial sediments to regional tectonic activity along the Min River in eastern Tibet

Wei Shi, Hanchao Jiang*, Siyuan Ma, Hongyan Xu, Jiawei Fan, Siqi Zhang

State Key Laboratory of Earthquake Dynamics, Institute of Geology, China Earthquake Administration, Beijing 100029, China

Corresponding author: Hanchao Jiang, E-mail: hcjiang@ies.ac.cn

Key Points:

- Three areas of tectonic activity are identified by analysis of the fluvial sediments from the Min River in eastern Tibet.
- The dominance of fluvial silts, low relief and low slope-angles indicate weak activity of the Minjiang fault.
- Stepwise increases in sands, relief, and slope-angle reveal increased tectonism in the Diexi-Wenchuan-Dujiangyan segments.

Abstract

The deposition of fluvial sediments in the tectonically active areas is mainly controlled by climate change and tectonic activity, meaning that fluvial sediments can provide a valuable record of regional climatic and tectonic signals. In this study, a detailed analysis was conducted on the grain-size of modern fluvial sediments from the upper Min River in eastern Tibet, and these data were combined with regional information about the vegetation, hydrology and geomorphology. The results indicate that modern regional tectonic activity in the study area can be divided into three segments. The fluvial sediments in Minjiangyuan-Diexi segment are dominated by fine silts (<63 m: 70.2%), showing low runoff and rainfall conditions and revealing a windblown origin influenced by climate change. This observation is consistent with the small hillslope angle and low relief in this segment, indicating weak activity of Minjiang fault. The coarse-grained fraction (>250 m) of fluvial sediments in Diexi-Wenchuan-Dujiangyan segments increases stepwise (A:6.2%, B:19.4%, C:33.8%) with a stable hydrological conditions, which corresponds well to the increasing trend in the regional relief and the steepness of hillslope angles. These observations indicate the phased enhancement of regional tectonic activity for Maoxian-Wenchuan fault. The fluvial sediments in Dujiangyan-Sichuan basin segment show good sorting and rounding, which is well correlated with significant increases in rainfall and runoff. There is also almost no evidence of tectonic activity in this segment. This study first develops an important research approach for revealing regional tectonic activity through fluvial sediment analysis in tectonically active regions.

Plain Language Summary

In tectonically active areas, intense tectonic activity tends to create steep geomorphology, and deeply affect erosion and sedimentation of river systems. Hence, whether fluvial sediments document changes of regional tectonic activity

deserve detailed investigation. In this study, the fluvial sediment of the Min River in the eastern Tibetan Plateau is taken as the research object. Based on grain size analysis of the Min River sediments, we reveal the close correlation between grain size variation and tectonic activity, under the comprehensive comparison of regional topography and geomorphology (slope, height difference) and hydrological conditions. We find that the fine-grained fluvial sediments from the Minjiangyuan to Diexi segment correspond to the weak fault activity of the Minjiang Fault, while the significant increase of coarse-grained composition from Diexi to Dujiangyan segment correspond to the enhancement of fault activity of the Maoxian-Wenchuan fault. This is supported by the greater slope angles and mountain relief from Diexi to Dujiangyan. Novelty of the research methods and reliability of results in this study provide a good reference for revealing regional tectonic activity through fluvial sediments in tectonically active areas.

Keywords: Modern fluvial sediments; Grain-size analysis; Tectonic activity; Upper Min River; Eastern Tibetan Plateau

1. Introduction

The provenance, transportation and deposition of terrigenous sediments are controlled by tectonic activity and climate change (e.g., Singh et al., 2007; Bravard et al., 2014). Clastic sediments are mainly transported by rivers, delivering material from the continents to the oceans (Milliman and Meade, 1983). Therefore, river sediments represent important archives of the Earth's geological history, recording the effects of tectonism and climate change.

Both the Yangtze River and the Yellow River originate from the Tibetan Plateau (TP). The northern and central parts of the TP have positive topography, while the eastern part is characterized by the largest relief and negative topography. Understanding the causes of these topographic patterns has been the subject of extensive scientific interest. The evolution of river systems and drainage efficiency has been proposed to systematically explain the regional landscape differences in the eastern TP (Liu et al., 2008). The Yangtze River system drains and removes sediment from the Sichuan Basin, possibly contributing to the relative increase in relief across the Longmen Shan region (Richardson et al., 2008). Accordingly, the evolution of river systems was possibly responsible for the high relief and negative topography in the eastern TP. Nevertheless, the gradient in precipitation across the eastern margin of the TP cannot fully explain the order of the magnitude differences in erosion, and river sediment data delineate a zone of relatively rapid denudation around active faults that contain the Longmen Shan in their hanging wall (Liu et al., 2011; Wang et al., 2021).

Strong earthquakes in active mountain belts can trigger landslides, which mobilize large volumes of clastic sediments (e.g., Keefer, 1994; Yin et al., 2009; Yin et al., 2010; Xu et al., 2012, 2014). The 2008 Wenchuan Ms 8.0 earthquake triggered >56, 000 landslides, covering a total area of >396 km^2 (Dai et al., 2011; Li et al., 2014; Xu et al., 2014). Delivery of these clastic sediments to

river channels may result in aggradation and flooding. Following the Wenchuan earthquake, suspended sediment discharge was elevated 3-7 times compared to the rates from 2006-2007 (Wang et al., 2015). The combination of coseismic landslide density and the frequency of intense runoff events appears to control the denudation, transportation, and deposition of clastic sediments (Hovius et al., 2011; Howarth et al., 2012; Wang et al., 2015). The entanglement of coseismic landslides and intense runoff events adds complexity to reconstructing the geomorphological evolution of tectonically active regions.

The Min River is one of the key tributaries of the Yangtze River and goes through the climate transition zone and the tectonically active region of the eastern TP. In this study, a suite of recently deposited river sediments was collected along the Min River, from the source to Dujiangyan (Figure 1). Detailed grain-size analyses were conducted with an aim to better understand and disentangle the various fluvial processes involved in the provenance, transport, and deposition of river sediments. This topic is of fundamental importance for Earth system science, involving the interactions between the lithosphere, biosphere, hydrosphere and atmosphere for the critical belts on the Earth.

2. Geographic and Geologic settings

Instrumental data since AD 1900 indicate that the TP has experienced strong earthquakes clustered around the Bayan Kala Block from 1995 to the present, known as the Kunlun-Wenchuan earthquake series (Deng et al., 2014). The eastern TP is characterized by alpine valleys and is controlled by the Longmen Shan thrust belts (including the Maoxian-Wenchuan fault, Yingxiu-Beichuan fault, and Jiangyou-Guanxian fault), the Minjiang fault and the Songpinggou fault (Figure 1a). Frequent tectonic activities have led to numerous earthquakes and landslides in this region (e.g., Zhang et al., 2003; Jiang et al., 2014; Li et al., 2015; Liang and Jiang, 2017), such as the 1933 Diexi M_s 7.5 earthquake, the 1976 Songpan M_s 7.2 earthquake, the 2008 Wenchuan M_s 8.0 earthquake and the 2017 Jiuzhaigou M_s 7.0 earthquake, which have caused geomorphological damages in this region. The GPS-measured uplift rates of the Longmen Shan fault zone reached 2-3 mm/yr over 10 years since 1999 (Liang et al., 2013). Thermochronological dating of zircon and apatite indicate denudation rates reaching 1-2 mm/y in the Longmen Shan region during the Late Cenozoic (Kirby et al., 2002).

The alpine valleys in the eastern TP leads to less preservation of the Quaternary sediments and a large area of outcropping bedrock. The bedrock exposed in the catchment region of the upper Min River is dominated by Silurian phyllite, quartz schist, and Triassic phyllite, metamorphic sandstone (Figure 1a), which are easily weathered and eroded into transportable debris (Zhong et al., 2019). Massive granites are also exposed in the study area. Among them, the Neoproterozoic Pengguan complex (U-Pb age: 859-699 Ma, Ma et al., 1996) (Figure 1a) is mainly composed of intermediate-acid intrusive rocks with small amounts of basic-ultrabasic intrusive rocks, volcanic rocks, volcanic clastic rocks and metamorphic rocks of greenschist facies. The coarse silt ($>$ 63 m) in the study

area has recently been demonstrated to have mainly derived from local debris material, probably related to dust storms linked to the loose surface material following earthquakes (Jiang et al., 2017; Liang and Jiang, 2017).

The upstream channel of the Min River (~260 km long) is aligned broadly N-S (Figure 1b), eroding the hinterland of the TP through the formation of gullies and valleys. The Min River valley is typically steep and narrow, with an incision depth of 800 m to 3000 m (e.g., Li et al., 2005; Zhang et al., 2005). The slopes on both sides of the study area are 18-45°, and the vertical aspect ratio of the valley is 5.5-12.6 ‰ (Zhang et al., 2005). Constrained by the specific landforms of alpine valleys, the wind direction in the study area is generally SSW/NNE, roughly consistent with the strike of local valleys (Liu, 2014). The Min River valley has high wind speeds in April (average 4.9 m/s) and low speeds in July (average 3.7 m/s). Wind speed is generally < 4 m/s before noon and > 4 m/s after noon, normally peaking at 16:00 at about 8-10 m/s, and the highest instantaneous wind speed in the study area reached 21 m/s (Liu, 2014).

The upper reaches of the Min River are located in the transition from the wet monsoon area to the high cold region of the TP. In this region, mean annual precipitation (MAP) ranges from 400 mm to 850 mm, and precipitation during the rainy season (May-October) is dominant (>75%) (Ding et al., 2014). It is noticeable that orographic rain in the eastern margin of the TP generates two storm areas, which are centered around Sandagu and Zipingpu (Figure 1b). The MAP of these regions is more than 1200 mm, based on the statistical analyses of precipitation data from 1982-2007 (Ding et al., 2014).

Regional vegetation has obvious vertical zonation, which mainly consists of small-leaf, arid shrubs (1300-2200 m a.s.l.), mixed broadleaf-conifer forests, evergreen and deciduous broad-leaved mixed forests (2000-2800 m a.s.l.), *Picea* and *Abies* forests (2800-3600 m a.s.l.), and alpine shrubs and meadows (> 3600 m a.s.l.) (Ma et al., 2004; Zhang et al., 2008). There are probably two key factors that greatly influence vegetation distribution and ecological conditions in the study area. One is an arid and windy climate with a large temperature difference between day and night. The other is active tectonics characterized by frequent earthquakes (Lin, 2008; Wang et al., 2011). Strong earthquakes often induce numerous landslides and destroy vegetation cover in the study area (Xu et al., 2012, 2014). These two factors make the landscape and vegetation fragile.

3. Materials and Methods

From the eastern TP (Minjiangyuan, 33°01 59 N, 103°42 42 E; 3462 m a.s.l.) to the Sichuan Basin (Dujiangyan, 30°56 25 N, 103°38 14 E; 634 m a.s.l.), 181 river samples were collected for grain size analysis at 25 sites (Table S1) from a ~265 km transect along the upper Min River during October 2017 (Figure 1b). Sampling sites were selected from exposed, freshly-developed depositional sequences close to the active channel and its margins (Figure 2). To ensure sample consistency associated with uniform flow regimes, each sample was collected at a depth of 0-0.2 m from different places of each sampling sequence. All locations

were carefully chosen to avoid contamination from riverbank materials or from anthropogenic reworking.

Grain-size analysis was conducted using a Malvern Master-sizer 3000 laser grain-size analyzer at the State Key Laboratory of Earthquake Dynamics, Institute of Geology, China Earthquake Administration in Beijing, China. About 0.5 g of sediment was pretreated with 20 ml of 30% H_2O_2 to remove organic matter and then with 10 ml of 10% HCl to remove carbonates. About 300 ml of deionized water was added, and the sample solution was kept for 24 h to rinse acidic ions. The sample residue was dispersed with 10 ml of 0.05 M $(NaPO_3)_6$ on an ultrasonic vibrator for 10 min before grain-size measurements. For each sample, the grain-size analyzer automatically outputs the median diameter (Md) and the percentages of each size fraction, with a relative error of less than 1%. SUS was measured using a Bartington MS2 susceptibility meter.

Numerical unmixing of grain-size distribution data into constituent components, known as end-member analysis (EMA), can yield valuable information on transport dynamics (Weltje et al., 1997; Paterson et al., 2015). We analyzed the Min River samples using the AnalySize software for processing and unmixing grain-size data (Paterson et al., 2015). Parameters were selected from the generalized Gaussian skewness model (SGG) (Egli, 2003).

Mean grain size (Ms), standard deviation ( ), skewness (Sk), and kurtosis (K_G) are commonly used to discriminate different depositional processes and environments. Sahu (1964) distinguished the aeolian processes from the littoral environment using the following equation:

$$Y = -3.5688\ Ms + 3.7016\ ^{2} - 2.0766\ Sk + 3.1135\ K_G \quad (1)$$

The Y values for all of the Lixian (Jiang et al., 2017) and Xinmocun (Jiang et al., 2014) samples are less than -2.74, indicating an aeolian provenance (Sahu, 1964).

4. Results

4.1 Segmented characteristics of the Min River

According to the topographical, geomorphic, faults and vegetation distribution, the upper Min River can be subdivided into 4 segments (Figure 1b).

Segment A: The Minjiangyuan - Diexi segment (3460-2190 m a.s.l.)

The riverbed in this segment is directly connected with one side of the Min Mountain and has a width of 2-150 m (Figure 2a). The relative relief of the Min Mountain increases significantly from Minjiangyuan to Diexi along the Min River. The vegetation coverage along this segment gradually deteriorates from *Picea*, *Abies*, shrubs and herbs in the Minjiangyuan - Songpan segment to a small number of shrubs and herbs in the Songpan - Diexi segment and the bedrock is obviously and widely exposed. In this region, the monthly maximum wind speed reaches 15.4 m/s in Songpan.

Segment B: The Diexi-Wenchuan segment (2190-1470 m a.s.l.)

In this segment, the riverbed width continuously decreases to only 30-50 m, and the Min mountains are always in direct contact with the riverbed of the Min River (Figure 2b). The longitudinal slope (12.6‰) reaches the maximum regional value (Zhang et al., 2005). The regional vegetation coverage is most sparse.

Segment C: The Wenchuan-Dujiangyan segment (1470-900m a.s.l.)

The riverbed width in this segment becomes wider to about 50-150 m (Figure 2c), and the regional vegetation is obviously improved. The hillside around the Zipingpu Reservoir is covered with thick broad-leaved trees and herbs. The monthly maximum wind speed in Lixian is 14.0 m/s.

Segment D: The Dujiangyan- segment (900 - 630 m a.s.l.)

This segment transitions into the middle reach of the Min River, and has flat geomorphological features. This segment shows the widest river valley (>200 m, Figure 2d). The monthly maximum wind speed reaches 13.8 m/s in Dujiangyan.

4.2 Characteristics of grain-size distribution and SUS

Figure 3 shows variations of the median grain size (Md), five grain-size fractions (0-2 m, 2-20 m, 20-63 m, 63-250 m, >250 m), SUS and Y values of the river sediments from the Min River. The grain-size distribution can be divided into four categories, corresponding to the different segments defined above. The average values of Md increased significantly at Diexi (from 31.0 to 80.8 m) and Wenchuan (from 49.3 to 170.2 m), and decreased slightly at Dujiangyan (from 220.4 to 119.2 m). Variations at these three sites are the most significant for the whole river (Figure 3).

Among them, segment A is mainly composed of the 2-20 m (26.4 - 62.2%, mean 40.3%) and 20-63 m (10.0 - 46.9%, mean 27.1%) fractions. The mean proportion of the > 63 m fraction is 29.9% (Figure 3), mainly contributed by the 63-250 m fraction (mean 23.7%). The >250 m fraction has a low mean value of 6.2%. The mean value of SUS is 11.6 (5.3-30.6), and the Y values vary from -12.8 to 17.3, among which 22 out of the 55 samples have Y values of less than -2.74.

Relative to segment A, the 63-250 m (21.4-69.9%, mean 34.6%) and >250 m (5.8-34.5%, mean19.4%) fractions in segment B increase significantly, and their mean proporions increase by 10.9% and 13.2%, respectively. On the contrary, the 2-20 m (3.8-36.7%, mean 25.3%) and 20-63 m (9.2-30.7%, mean 20.3%) fractions decrease significantly by 15.0% and 6.8%, respectively. SUS values vary from 7.1 to 21.9 with a mean value of 12.4.

Md in segment C varies between 396.9 m and 2083.8 m and has the largest mean value (800.0 m) of the whole Min River (Figure 3) because the proportion of the > 250 m (9.1-55.7%) fraction reaches the highest with the mean value of 33.8%. On the contrary, the c proportion of the 2-20 m (6.4-32.5%, mean 20.0%) and 20-63 m (8.3-22.3%, mean 13.9%) fractions decrease further. The

63-250 m (11.9-50.3%, mean 31.9%) fraction remain stable. Intriguingly, the SUS values in segment C increase to the highest values (28.5-546.5) (Figure 3) near the location of the Pengguan complex (Figure 1a), with an abnormally high mean of 227.3. These values are much higher than the SUS values of the other river segments (mean 11.5). The Y values of segments B and C are all greater than -2.74.

In segment D, the 63-250 m content (45.6 - 67.0%) reaches the highest with the mean of 59.5% (Figure 3f). In contrast, the 2-20 m (10.0 - 17.3%, mean 13.0%) and 20-63 m (5.5 - 13.7%, mean 9.5%) decrease to the lowest, and >250 m (5.1 - 33.2%, mean 17.5%) fractions decrease significantly. SUS values vary from 142.1 to 356.5 with a mean value of 251.8. The Y values of segment D are completely greater than -2.74.

4.3 End-element analysis (EMA)

In sedimentology, EMA is often used to reveal information on provenance and transport dynamics (Weltje, 1997; Paterson and Heslop, 2015; Jiang et al., 2017). Three end-members (EMs) ($R^2 = 0.93$) are obtained from the Min River samples (Figure 4), and their peaks concentrate in the 21.2 m (58.0%), 185.8 m (24.2%) and 351.7 m (17.8%) ranges. EM_1 probably represents background and regional dust (Dietze et al., 2014; Jiang et al., 2017), while EM_2 represents the component of river transport (Middleton, 1976; Tsoar and Pye, 1987; Bennett and Best, 1995; Yin et al., 2009; Sun et al., 2002) because the Min River has water all year round, although with low runoff. EM_3 represents the local component transported by rolling and jumping because the riverbed of the upper Min River extends along the Min mountains.

Along the upper Min River downwards, three EMs show obvious stepwise changes (Figure 5). EM_1 content shows a stepwise decrease (a: 82.5% b: 53.1% c: 38.6% and d: 23.7%), corresponding to the sum of the 2-20 m and the 20-63 m fractions (Figure 3, 5). EM_2 varies like that of the 63-250 m fraction, showing a sudden increase from segment A to B (from 13.1% to 31.4%), and segment C to D (from 27.1% to 67.4%), and a relatively stable fluctuation from segment B to C (31.4% and 27.1%). EM_3 corresponds to the >250 m fraction (Figure 3, 5), showing a stepwise increase from segment A to B to C (4.4%, 15.5% and 38.6%), and a significant decrease from segment C to D (from 38.6 to 23.7%).

The mode number of grain-size frequency distribution can be used to reflect the number of sediment sources (McKinney and Sanders, 1978). The grain-size frequency distribution of river samples from segment A presents a discrete feature, mainly concentrated in the ~11.8 m, ~48.8 m and ~177.2 m fractions (Figure 4). The mode value of the ~48.8 m fractions is the main peak and represents the dust source transported by wind. The modes of the weak ~11.8 m and ~177.2 m peaks (Figure 5) represent background dust and local fluvial transport components, respectively. The grain-size frequency distribution of segments B and C shows a highly concentrated bimodal model (Figure S1).

The mode values of the ~203.1 m and ~270.4 m fractions are the dominant peaks for segment B and C, respectively, and represent the local rolling and jumping (major) and fluvial transport (minor), given the aridity, low runoff and close correspondence of SUS to the local lithology at Wenchuan (Figure 3). The minor peaks concentrate at ~17.0 m and ~18.9 m for segments B and C, respectively, and represent background and regional dust transported by wind. The grain-size frequency of segment D shows a concentrated unimodal distribution (Figure S1), with the mode value of ~171.4 m representing the fluvial transport component given the generally good sorting and rounding.

4.4 Analysis of C-M, F-M diagrams

C (one-percentile proportional) - M (median diameter), and F (weight percentage of fraction <125 m) - M diagrams are often used to reveal information about transport dynamics (Passega, 1957; Singh et al., 2007). In the C-M diagram, the samples in segment A are completely separated from those in segments C and D. Most samples in segment B are distributed with those of segment C (Figure 6a). The M value in segment A (13.9-89.8 m) (Figure 3) is mainly distributed in the RS section (Figure 6a), indicating uniformly suspended deposition in the river (Passega, 1957). Specifically, the strong wind (15.4 m/s) at high altitudes (3460-2190 m, mean: 2840 m) transports the dust fractions into the Min River, though the C values widely fluctuate between 54.8 and 964.3 m (Figure 6a). The samples of segment B distribute discretely in the P-Q-R section, reflecting mixed transportation including rolling and jumping components, fluvial transport components and uniformly suspended components (Figure 6a), with C values of 383.5-1066.0 m and M values of 32.2-171.4 m. The samples of segment C are concentrated in the PQ section (Figure 6a), reflecting rolling and jumping transportation (Passega, 1957), with C values of 396.9-2083.8 m and M values of 70.3-319.1 m. The samples in segment D are close to the RQ section and are distributed parallel to the C = M line, which reflects the graded suspension transport of riverbed sediments (Figure 6a) (Singh et al., 2007). The distribution of samples in different segments along the Min River in the F-M diagrams show similar features to the C-M diagrams (Figure 6).

5. Discussion

The variability of grain-size components in fluvial sediments is influenced by provenance supply and transport dynamics (Passega, 1957; Singh et al., 2007; Dietze et al., 2014). The various mode values, as well as the proportions of various grain-size fractions and EMs, reflect the distinct provenance of the fluvial sediments in different segments along the Min River (McKinney and Sanders,1978; Sun et al., 2002; Sun et al., 2007; Dietze et al., 2014; Vandenberghe, 2013). The distribution of river samples in the C-M and F-M diagrams reflect different transportation and depositional processes (Passega, 1957).

5.1 Segment A - Fine-grained fluvial sediments dominated by the climate

The <63 m fraction (70.2%) in segment A corresponds to the proportional

changes of EM_1 (21.2 m: 82.5%). Previous studies indicate that the 10-40 m components represent background and regional dust transported by wind (Jiang et al., 2014 2017), which contribute to 51± 11% and 42±14% of the lacustrine sediments across the TP, respectively (Dietze et al., 2014). Generally, similar EMs reflect similar provenance and depositional processes of sediments (Sun et al., 2002, 2004; Dietze et al., 2014; Vandenberghe,2013). In this study, the fine-grained fractions in segment A indicate an aeolian provenance. This finding is supported by five lines of evidence: 1) Md varies within a narrow range from 13.9 to 89.8 m, though the C values fluctuate widely between 54.8 and 964.3 m (Figure 6a); 2) The samples distribution in the RS section in the C-M diagram (Figure 4) reflect uniform suspension, probably transported by wind (Passega, 1957); 3) Nearly half of the samples (22/total 55) have Y values of less than -2.74, which is indicative of an aeolian origin (Sahu, 1964); 4) Loess has accumulated widely in the study area (Liu et al., 2013; Shen et al., 2017) and can supply an adequate source of dust particles; 5) the study area has a high mean altitude of 2840 m, and the monthly maximum wind speed reaches 15.4 m/s, which provides additional evidence for strong aeolian transport.

The study area is dominated by a windy and semi-arid climate (Jiang et al., 2014). The relatively low precipitation (400-700 mm/a) and low runoff (18.4-43.4×10^8 m^3) (Figure 1b) in segment A reflect the limited river transport capacity. In segment A, the hillslope angle (5°-34.8°) and local relief (243-1572 m) gradually increase along the Min Mountains, especially from Zhenjiangguan to Diexi (Figure 7d, e), indicating the enhancement of the river erosion with the decrease of altitude (from 3460 to 2190 m). These features are consistent with the low fault activity of the Minjiang Fault from Minjiangyuan to Songpan (0.30-0.53 mm/a, Zhou et al., 2000, 2006; Tan et al., 2019). Due to the low tectonic activity in this region and consequently a weak influence on the supply of local provenance (Jiang et al., 2014, 2017), the fluvial sediments in segment A contain low contributions of EM_2 and EM_3.

5.2 Segments B and C - Coarse-grained deposition controlled by tectonism

The >250 m fraction in segment B and C are significantly higher, compared with that of segment A. The proportion of this component increases stepwise from segment B to C until it reaches the maximum value of the whole sequence. The 63-250 m fraction increases suddenly in the transition from segment A to B and then shows relatively stable fluctuations (Figure 3). In contrast, the proportion of the fine (<63 m) windblown fraction shows a gradual decrease (Figure 3, 5). The C-M, F-M and EMA analyses results show that, from segment B to C, the suspended component decreases (EM_2), while the rolling and jumping component (EM_3) increases (Figure 3, 5).

Notably, Segment B begins at the intersection of the Minjiang Fault and the Songpinggou Fault (Figure 1a), the epicenter of the Diexi *M* 7.5 earthquake in 1933 (Chen et al., 1994; Ren et al., 2018). Field surveys show that the altitude decreases by 400 m within a horizontal distance of 20 km downstream from

Diexi, so that both the longitudinal slope of the riverbed (12.6‰, Figure 7c, Zhang et al., 2005) and the hillslope angle (41.4°, Figure 7d) all reach the maximum value of the whole area studied. These remarkable changes of geomorphic features correspond well to a twofold increase in erosion coefficients within 15 km of major faults in the eastern TP (Kirkpatrick et al., 2020) and the more intense denudation at the location of seismogenic faulting along high-relief plateau margins (Li et al., 2017). In addition, the rapid increase of the base-level of the Min River in segment B causes enhancement of the river's cutting and transport capacity (Merritts and Vincent, 1989; Cheng et al., 2004).

In segment B, the hillslope angle (12.3-41.4°, mean 30.1°) is generally greater than the average of the whole study area (25.1°), and the highest angles (41.4°) are far over the stability threshold of ~32° for landslide denudation (Burbank, et al., 1996; Clarke and Burbank, 2010; Montgomery and Brandon, 2002). The relatively low hillslope angles in segment B reflect that landslide dominated hillslope denudation has kept pace with rates of rock uplift and valley incision (Burbank, et al., 1996; Clarke and Burbank, 2010; Montgomery and Brandon, 2002). That is to say, landslides in the upper reach of the Min River are probably driven by tectonic activity (Li et al., 2015; Jiang et al., 2014).

Local relief in segment B increases first and then decreases (Figure7c). Correspondingly, the flow direction of the Min River changes from roughly N-S to NW-SE in segment B (Figure 1a). The lithology also changes from Triassic (phyllite and metamorphic sandstone) to Silurian (phyllite, quartz schist) (Figure 1a), and faulting transforms from the Minjiang fault to the Maoxian-Wenchuan fault. This transformation of tectonic activity and the lithology play a controlling role on fluvial erodibility (Zondervan et al., 2020) and influence regional geomorphology and river drainage, given that annual rainfall in segment B is the lowest (less than 500 mm/a, Figure 1) in the study area.

Overall, in segment B, the outcropping bedrock suffered severe damage due to tectonic activity and provided fresh local sediment sources (EM_3). The narrower valley and the direct contact between the riverbed and hillside on either side in segment B (Figure 2b) provide favorable conditions for rolling and jumping transportation along the hillslope. The absence of Quaternary loose sediments causes a significant decrease in background dust deposition (EM_1).

The proportion of the >250 m fraction reaches the maximum value in segment C and shows drastic fluctuation, which causes the maximum values of C and M (Figure 7a, b). Intriguingly, the SUS values in segment C increase to abnormally high values (28.5-546.5, mean: 227.3) near the exposure of the Pengguan complex (Figure 3), but lower SUS values appear in the surrounding area (Zagunao River: 9.1-114.1, mean 34.1, Figure S2; Zipingpu reservoir: 5-60, Zhang et al., 2019; Segment A and B: 5.3-30.6, mean 11.5, Figure 3). Noticeably, the precipitation in segment C is still low (400-700 mm/a) and only significantly increase near the Zipingpu reservoir (1200 mm/a) (Figure 1B). In addition, the grain size (mean 170.2 m) of segment C increases before the Zagunao River (mean 83.1 m, Figure S2) joins the Min River (Figure 1b, Figure 3). Therefore,

the abnormally high values of grain size and SUS in segment C are caused by a provenance change rather than the climate.

> Tectonically, the Maoxian-Wenchuan fault mainly controls the distribution of the Min River in segment C (Figure1). This fault has a large dextral slip rate (1.0-3.8mm /a; Chen and Li 2013 Wang et al., 2017) and a large vertical slip rate (~1-2 mm/a; Liu et al., 2015). Previous studies show that the Maoxian-Wenchuan fault is distributed on the maximum exhumation belt along the eastern Longmen Shan fault zone (Tan et al., 2019). Therefore, the rapid regional uplift and denudation (Kirby et al., 2002 Liang et al., 2013) not only caused a larger hillslope angle (mean 24.9°) and the highest local relief (2188 m) but also provided widespread fresh coarse-grained local sediment sources in segment C of the Min River basin (Figure 7 d, e).

The regional bedrock is dominated by the harder Pengguan complex (Mesozoic granites) (Figure 1a). The increasing trend of the slope angle and local relief along segment C indicate that the active Maoxian-Wenchuan fault (Tan et al., 2019) led to the enhancement of rock uplift and valley incision. However, the increase in bedrock strength of the Pengguan complex will have modulated the slope threshold (mean hillslope angle of 24.9°) (Molnar et al., 2007; Clarke and Burbank et al., 1996). The high hillslope angle and local relief in segment C provide prime conditions for rolling and jumping transport of the coarse local component (EM_3), which corresponds to the PQ distribution in the C-M diagram (Figure 4) (Passega, 1957). The exposed harder Mesozoic granites provides coarser local components that correspond to the maximum M and C values. Although regional climate generally has a weak influence on coarse particles supply, the concentrated distribution of grain-size frequency (Figure 2c) indicates that fluvial action played an effective role in sorting of local sediment sources (Sun et al.,2002; Sahu, 1964; Frings, 2008).

Generally, the large earthquake was followed by a period of enhanced mass wasting and fluvial sediment evacuation (Hovius et al., 2011; Dadson et al., 2004; Wang et al., 2015). The Wenchuan *M*s 8.0 earthquake in 2008 caused serious geomorphic damage, and the annual average suspended sediment flow in regional rivers increased 3-7 times after the earthquake. The river recovered to the pre-earthquake level 1.2 ± 0.9 years later (Wang et al., 2015). However, over 70% of the co seismic debris has stabilized in place along the hillslopes after ten years (Dai et al., 2021) and will take 370 years to remove (Wang et al., 2017). Accordingly, we believe that coseismic debris caused by the Wenchuan earthquake in 2008 had little influence on our sample collection in 2017. In this study, the >250 m fraction in segment B and C represent a local sediment source transported by rolling and jumping along the hillslope, corresponding to EM_3. The stronger tectonic activity in segment C than that in segment B is the main driving force controlling the increase of the coarse grain-size.

5.3 Segment D - typical river sediments

In segment D, the proportion of the 63-250 m fraction reaches the highest value (59.5%) of the whole sequence, corresponding to the maximum value of EM_2 (185.8 m: 67.4%). This finding is consistent with previous studies showing that fluvial deposits are composed mainly a medium-sand component (modal size: 200-400 m) (Middleton, 1976; Tsoar and Pye, 1987 Bennett and Best, 1995). In addition, the single peak mode (174.1 m, Figure 5) of segment D represents a single river transport process and sedimentary environment. In the C-M diagram, the distribution of river samples adjacent to the C=M line reflects the suspension transport of riverbed sediments (Figure 5a) (Singh et al., 2007 Passega, 1957). The concentrated distribution of grain-size frequency also reflects a well-sorted product of fluvial action (Sun et al., 2002).

Segment D is located on the interior of the Sichuan Basin, completely free from the influence of alpine valleys in the eastern TP, and is characterized by a wide and flat geomorphological surface (Figure 2d). The gravels on the riverbed are very well rounded due to extensive river scouring, and the samples in this study were collected between the large gravels (Figure 2d). Because the Zipingpu reservoir captures amounts of sediments, especially from the >250 m component (Figure 3), the EM_3 and C values in segment D decreased sharply (Figure 5, 7). This finding explains the river's selective transport in downstream fining processes (Frings, 2008). Therefore, the characteristic of sediments in segment D mainly reflects the typical fluvial sediments (EM_2).

6. Conclusion

Grain-size analysis was conducted on modern fluvial sediments of the upper Min River and integrated with vegetation, hydrology, geomorphology (relief and hillslope) and geology (fault and bedrock) data to extract regional climate and tectonic signals in the eastern TP. Three areas of tectonic activity along the upper Min River are identified. The Minjiang fault (Minjiangyuan-Diexi) generally shows weak activity. Two segments from Diexi to Wenchuan and from Wenchuan to Dujiangyan show the phased enhancement of regional tectonic activity. The segment from Dujiangyan to the Sichuan basin reveals almost no evidence of tectonic activity.

Acknowledgments

This study was supported by the National Nonprofit Fundamental Research Grant of China, Institute of Geology, China Earthquake Administration (IGCEA2126 and IGCEA1906). Data are available in the figshare database (https://doi.pangaea.de/10.6084/m9.figshare.17111402).

References

Bennett, S.J. & Best, J.L. (1995). Mean flow and turbulence structure over fixed, two dimensional dunes: implications for sediment transport and bedform stability. Sedimentology, 42(3), 491-513. https://doi.org/10.1111/j.1365-3091.1995.tb00386.x

Bravard, J.P., Goichot, M. & Tronchère, H. (2014). An assessment of sediment-transport processes in the Lower Mekong River based on deposit grain sizes, the CM technique and flow-energy data. Geomorphology, 207(feb.15), 174-189. https://doi.org/10.1016/j.geomorph.2013.11.004

Burbank, D.W., Fielding, E., Anderson, R.S., Brozovic, N., Reid, M. D.C. & Leland, J. (1996). Bedrock incision, rock uplift and threshold hillslopes in the northwestern Himalayas. Nature, 379(6565), 505-510. https://doi.org/10.1038/379505a0

Chen, H. & Li, Y. (2013). Water system responding to the dextral strike-slipping of the Longmen Shan fault zone in the upper Min River basin. Journal of Mountain Science, 31(2),211-217 (in Chinese).

Chen, S.F., Wilson, C., Deng, Q.D., Zhao, X.L. & Zhi, L.L. (1994). Active faulting and block movement associated with large earthquakes in the Min Shan and Longmen Mountains, northeastern Tibetan Plateau. Journal of Geophysical Research: Solid Earth, 99(B12), 24025-24038. https://doi.org/10.1029/94JB02132

Cheng, S.P., Deng, Q.D., Li, C.Y. & Yang, G.Z. (2004). Dynamical mechanism, physical erosion processes and influence factors of fluvial incision A review and prospect. Quaternary Sciences, 24(4), 421-429 (in Chinese).

Clarke, B.A. & Burbank, D.W. (2010). Bedrock fracturing, threshold hillslopes, and limits to the magnitude of bedrock landslides. Earth and Planetary Science Letters, 297(3-4),577-586. https://doi.org/10.1016/j.epsl.2010.07.011

Dadson, S.J., Hovius, N., Chen, H., Dade, W.B., Lin, J.C., Hsu, M.L., Lin, C.W., Horog, M.J., Chen, T.C., Milliman, J. & Stark, C.P. (2004). Earthquake-triggered increase in sediment delivery from an active mountain belt. Geology, 32(8),733-736. https://doi.org/10.1130/G20639.1

Dai, F.C., Xu, C., Yao, X., Xu, L., Tu, X.B. & Gong, Q.M. (2011). Spatial distribution of landslides triggered by the 2008 Ms 8.0 Wenchuan earthquake, China. Journal of Asian Earth Sciences, 40(4), 883-895. https://doi.org/10.1016/j.jseaes.2010.04.010

Dai, L.X., Scaringi, G., Fan, X.M., Yunus, A.P., Liu-Zeng, J., Xu, Q. & Huang, R.Q. (2021). Coseismic debris remains in the orogen despite a decade of enhanced landsliding. Geophysical Research Letters. https://doi.org/10.1029/2021GL095850

Deng, Q.D., Cheng, S.P., Ma, J. & Du, P. (2014). Seismic activities and earthquake potential in the Tibetan Plateau. Chinese Journal of Geophysics, 57(5), 2025-2042 (In Chinese).

Dietze, E., Maussion, F., Ahlborn, M., Diekmann, B., Hartmann, K., Henkel, K., Kasper, T., Lockot, G., Opitz, S. & Haberzettl, T. (2014). Sediment transport processes across the Tibetan Plateau inferred from robust grain-size end

members in lake sediments. Climate of the Past 10, 91-106. https://doi.org/10.5194/cp-10-91-2014

Ding, H.R., Ma, G.W., Ni, S.J., Shi, Z.M., Zhao, G.H., Yan, L. & Yan, Z.K. (2014) Study on sediment discharge increase caused by Wenchuan earthquake landslide and heavy rainfall in the upper reaches of the Min River. Journal of Sichuan University, 46(3), 49-55 (in Chinese).

Egli, R. (2003). Analysis of the field dependence of remanent magnetization curves. Journal of Geophysical Research Solid Earth, 108(B2), 1-26. https://doi.org/10.1029/2002JB002023

Frings, R.M. (2008). Downstream fining in large sand-bed rivers. Earth Science Reviews, 87(1-2), 39-60. https://doi.org/10.1016/j.earscirev.2007.10.001

Hovius, N., Meunier, P., Lin, C.W., Chen, H., Chen, Y.G., Dadson, S., Horng, M.J. & Lines, M. (2011). Prolonged seismically induced erosion and the mass balance of a large earthquake. Earth and Planetary Science Letters, 304(3-4), 347-355. https://doi.org/10.1016/j.epsl.2011.02.005

Howarth, J.D., Fitzsimons, S.J., Norris, R.J. & Jacobsen, G.E. (2012). Lake sediments record cycles of sediment flux driven by large earthquakes on the Alpine fault, New Zealand. Geology, 40(12), 1091-1094. https://doi.org/10.1130/G33486.1

Jiang, H.C., Mao, X., Xu, H.Y., Yang, H.L., Ma, X.L., Zhong, N. & Li, Y.H. (2014). Provenance and earthquake signature of the last deglacial Xinmocun lacustrine sediments at Diexi, East Tibet. Geomorphology, 204(jan.1), 518-531. https://doi.org/10.1016/j.geomorph.2013.08.032

Jiang, H.C., Zhong, N., Li, Y.H., Ma, X.L., Xu, H.Y., Shi, W., Zhang, S.Q. & Nie, G.Z. (2017). A continuous 13.3-ka record of seismogenic dust events in lacustrine sediments in the eastern Tibetan Plateau. Scientific Reports, 7:15686. https://doi.org/10.1038/s41598-017-16027-8

Keefer, D.K. (1994). The importance of earthquake induced landslides to long-term slope erosion and slope-failure hazards in seismically active regions. Geomorphology, 10(1), 265-284. https://doi.org/10.1016/0169-555X(94)90021-3

Kirby, E., Reiners, P.W., Krol, M.A., Whipple, K.X., Hodges, K.V., Farley, K.A., Tang, W.Q. & Chen, Z.L. (2002). Late Cenozoic evolution of the eastern margin of the Tibetan Plateau: inferences from 40Ar/39Ar and (U-Th)/He thermochronology. Tectonics, 21(1), 1-20. https://doi.org/10.1029/2000TC001246

Kirkpatrick, H.M., Moon, S., Yin, A. & Harrison, T.M. (2020). Impact of fault damage on eastern Tibet topography. Geology, 49(1). https://doi.org/10.1029/2000TC001246

Li, G., Joshua West, A., Densmore, A.L., Jin, Z.D., Parker, R.N. & Hilton, R.G. (2014). Seismic mountain building: Landslides associated with the 2008

Wenchuan earthquake in the context of a generalized model for earthquake volume balance. Geochemistry Geophysics Geosystems, 15(4), 833-844. https://doi.org/10.1002/2013GC005067

Li, G., Westa, A.J., Densmoreb, A.L., Jin, Z.D., Zhang. F., Wang, J., Clark, M. & Hilton, R.G. (2017). Earthquakes drive focused denudation along a tectonically active mountain front. Earth and Planetary Science Letters, 472, 253-265. https://doi.org/10.1016/j.epsl.2017.04.040

Li, Y., Cao, S.Y., Zhou, R.J., Densmore, A.L. & Ellis, M. (2005). Late Cenozoic Minjiang incision rate and its constraint on the uplift of the eastern margin of the Tibetan plateau. ACTA Geologica SINICA, 79(1), 28-37. https://doi.org/10.1007/s10409-004-0010-x

Li, Y.H., Jiang, H.C., Xu, H.Y. & Liang, L.J. (2015). Analyses on the triggering facrors of large quantities of landslides in the upper reaches of the Minjiang River, Sichuan province. Seismology and Geology, 37(4), 1147-1161(in Chinese).

Liang, L.J. & Jiang, H.C. (2017). Geochemical composition of the last deglacial lacustrine sediments in east Tibet and implications for provenance, weathering, and earthquake events. Quaternary International, 430(PT. B), 41-51. https://doi.org/10.1016/j.quaint.2015.07.037

Liang, S.M., Gan, W.J., Shen, C.Z., Xiao, G.R., Liu, J., Chen, W.T., Ding, X.G. & Zhou, D.M. (2013). Three-dimensional velocity field of present-day crustal motion of the Tibetan Plateau derived from GPS measurements. Journal of Geophysical Research: Solid Earth, 118(10), 1-11. https://doi.org/10.1002/2013JB010503

Liu, M. (2014). Research on the risk stone under wind loading with wind tunnel test in the Min River Valley. Chengdu University of Technology, Sichuan, 1-95 (in Chinese).

Lin, M.B. (2008). The huge Wenchuan earthquake and Longmen tectonic belt. Journal of Chengdu University of Technology, 35(4), 366-370 (in Chinese).

Liu, W.M., Yang, S.L. & Fang, X.M. (2013). Loess recorded climatic change during the last glaciation on the eastern Tibetan Plateau, western Sichuan. Journal of Jilin University (Earth Science Edition), 43(3), 974-982.

Liu, X.X., Wu, Y.Q., Jiang, Z.S., Zhan, W., Li, Q., Wen, W.X. & Zhou, Z.Y. (2015). Preseismic deformation in the seismogenic zone of the Lushan Ms 7.0 earthquake detected by GPS observations. Science in China (Earth Sciences), 45(9),1198-1207. https://doi.org/10.1007/s11430-015-5128-0

Liu, Z.J., Tapponnier, P., Gaudemer, Y. & Ding, L. (2008). Quantifying landscape differences across the Tibetan Plateau: Implications for topographic relief evolution. Journal of Geophysical Research, 113, F04018. https://doi.org/10.1029/2007JF000897

Liu, Z.J., Wen, L., Oskin, M. & Zeng, L.S. (2011). Focused modern denudation

of the Longmen Shan margin, eastern Tibetan Plateau. Geochemistry Geophysics Geosystems 12(11), Q11007. https://doi.org/10.1029/2011gc003652

Ma, K.M., Fu, B.J., Liu, S.L., Guan, W.B., Liu, G.H., Lu, Y.H. & Anand, M. (2004). Multiple-scale soil moisture distribution and its implications to ecosystem restoration in an arid river valley, China. Land Degradation and Development, 15(1), 75-85. https://doi.org/10.1002/ldr.584

Ma, Y.W., Wang, G.Z. & Hu, X.W. (1996). Tectonic deformation of Pengguan complex as a nappe. Acta Geologica Sichuan, (2), 110-114 (in Chinese).

McKinney, G.M. & Sanders, J.E. (1978). Principles of sedimentology. Wiley, New York, No. of pages 792.

Merritts, D. & Vincent, K.R. (1989). Geomorphic response of coastal streams to low, intermediate, and high rates of uplift, Medocino triple junction region, northern California. Geological Society of America Bulletin, 101,1373-1388. ht tps://doi.org/10.1130/0016-7606(1989)101<1373:GROCST>2.3.CO;2

Middleton, G.V. (1976). Hydraulic interpretation of sand size distributions. Journal of Geology, 84(4), 405-426. https://doi.org/10.2307/30066059

Milliman, J.D. & Meade, R.H. (1983). World-wide delivery of river sediments to oceans. Journal of Geology 91, 1-9. https://doi.org/10.1086/628741

Molnar, P., Anderson, R.S. & Anderson, S.P. (2007). Tectonics, fracturing of rock, and erosion. Journal of Geophysical Research Earth Surface, 112, F03014. https://doi.org/10.1029/2005JF000433

Montgomery, D.R. & Brandon, M. T. (2002). Topographic controls on erosion rates in tectonically active mountain ranges. Earth and Planetary Science Letters, 201(3), 481-489. https://doi.org/10.1016/S0012-821X(02)00725-2

Passega, R. (1957). Texture as characteristic of clastic deposition. American Association of Petroleum Geologists, 41, 1952-1984. https://doi.org/10.1306/0BDA594E-16BD-11D7-8645000102C1865D

Paterson, G.A. & Heslop, D. (2015). New methods for unmixing sediment grain size data. Geochemistry Geophysics Geosystems, 16(12), 4494-4506. https://doi.org/info:doi/10.1002/2015GC006070

Ren, J.J, Xu, X.W., Zhang, S.M., Yeats, R. S., Chen, J.W., Zhu, A.L. & Liu, S. (2018). Surface rupture of the 1933 Ms 7.5 Diexi earthquake in eastern Tibet: implications for seismogenic tectonics. Geophysical Journal International, 212(3), 627-1644. https://doi.org/10.1093/gji/ggx498

Richardson, N.J., Densmore, A.L., Seward, D., Fowler, A., Wipf, M., Ellis, M.A., Yong, L. & Zhang, Y. (2008). Extraordinary denudation in the Sichuan basin: Insights from low-temperature thermochronology adjacent to the eastern margin of the Tibetan Plateau, Journal of Geophysical Research, 113, B04409. https://doi.org/10.1029/2006jb004739

Sahu, B. K. (1964). Depositional mechanisms from the size analysis of clastic sediments. Journal of Sedimentary Research, 34, 73-83. https://doi.org/10.1306/74D70FCE-2B21-11D7-8648000102C1865D

Shen, Y.Q., Guo, C.B., Wu, R.A., Ren, S.S., Su, F.R. & Zhang, T. (2017). Analysis on the development characteristics and engineering geomechanical properties of the Songpan loess, western Sichuan province, China. Journal of Geomechanics, 23(5), 131-142(in Chinese).

Singh, M., Singh, I.B. & Müller, G. (2007). Sediment characteristics and transportation dynamics of the Ganga River. Geomorphology, 86(1/2), 144-175. https://doi.org/10.1016/j.geomorph.2006.08.011

Sun, D.H., Bloemendal, J., Rea, D.K., An, Z.S., Vandenberghe, J., Lu, H.Y., Sun, R.X. & Liu, T.S. (2004). Bimodal grain-size distribution of Chinese loess, and its palaeoclimatic implications. Catena, 55(3), 325-340. https://doi.org/10.1016/S0341-8162(03)00109-7

Sun, D.H., Bloemendal, J., Rea, D.K., Vandenberghe, J., Jiang, F.C., An, Z.S. & Su, R.X. (2002). Grain-size distribution function of polymodal sediments in hydraulic and aeolian environments, and numerical partitioning of the sedimentary components. Sedimentary Geology, 152(3-4), 263-277. https://doi.org/10.1016/S0037-0738(02)00082-9

Sun, J.M, Li, S.H., Muhs, D. R. & Li, B. (2007). Loess sedimentation in Tibet: provenance, processes, and link with Quaternary glaciations, Quaternary Science Reviews, 26(17-18), 2265-2280. https://doi.org/10.1016/j.quascirev.2007.05.003

Tan, X.B., Liu, Y.D., Lee, Y.H., Lu, R.Q., Xu, X.W., Suppe, J., Shi, F. & Xu, C. (2019). Parallelism between the maximum exhumation belt and the Moho ramp along the eastern Tibetan Plateau margin: Coincidence or consequence?. Earth and Planetary Science Letters, 507,73-84. https://doi.org/10.1016/j.epsl.2018.12.001

Tsoar, H. & Pye, K. (1987). Dust transport and the question of desert loess formation, Sedimentology, 34(1), 139-153. https://doi.org/ 10.1111/j.1365-3091.1987.tb00566.x/full

Vandenberghe, J., Lu, H., Sun, D., Huissteden, J. & Konert, M. (2004). The late Miocene and Pliocene climate in East Asia as recorded by grain size and magnetic susceptibility of the Red Clay deposits (Chinese Loess Plateau). Palaeogeography Palaeoclimatology Palaeoecology, 204(3-4), 239-255. https://doi.org/10.1016/S0031-0182(03)00729-6

Wang, J., Jin, Z.D., Hilton, R.G., Zhang, F., Densmore, A.L., Li, G. & West A.J. (2015). Controls on fluvial evacuation of sediment from earthquake-triggered landslides. Geology, 43(2), 115-118. https://doi.org/10.1130/G36157.1

Wang, P., Zhang, B., Qiu, W.L. & Wang, J.C. (2011). Soft-sediment deformation structures from the Diexi paleo-dammed lakes in the upper reaches of the

Minjiang River, east Tibet. Journal of Asian Earth Sciences, 40(4), 865-872. https://doi.org/10.1016/j.jseaes.2010.04.006

Wang, W., Godard, V., Liu-Zeng, J., Scherler, D., Xu, C., Zhang, J.Y., Xie, K.J., Bellier, O., Ansberque, C., Sigoyer, J. & Team, A. (2017). Perturbation of fluvial sediment fluxes following the 2008 Wenchuan earthquake. Earth Surface Processes and Landforms, 42(15), 2611-2622. https://doi.org/10.1002/esp.4210

Wang, W., Godard, V., Liu-Zeng, J., Zhang, J.Y., Li, Z.G., Xu, S., Yao, W.Q. & Yuan, Z.D., Aumaître, G., Bourlès, D.L., Keddadouche, K. (2021). Tectonic controls on surface erosion rates in the Longmen Shan, eastern Tibet. Tectonics, 40(3). https://doi.org/10.1029/2020TC006445

Wang, X.G., Li, C.Y., Lu, L.X. & Dong, J.B. (2017). Analysis of the late Quaternary activity along the Wenchuan-Maoxian fault-middle of the back- range fault at the Longmen Shan fault zone. Seismology and Geology, 39(3), 572-586. https://doi.org/10.3969/j.issn.0253-4967.2017.03.010

Weltje, G.L. (1997). End-member modeling of compositional data: Numerical-statistical algorithms for solving the explicit mixing problem. Mathematical Geology, 29(4), 503-549. https://doi.org/10.1007/BF02775085

Xu, C., Xu, X.W., Dai, F.C., Xiao, J.Z., Tan, X.B. & Yuan, R.M. (2012). Landslides hazard mapping using GIS and weight of evidence model in Qingshui River watershed of 2008 Wenchuan earthquake struck region. Journal of Earth Science, 23(1), 97-120. https://doi.org/CNKI:SUN:ZDDY.0.2012-01-010

Xu, C., Xu, X.W., Yao, X. & Dai, F.C. (2014). Three (nearly) complete inventories of landslides triggered by the May 12, 2008 Wenchuan Mw 7.9 earthquake of China and their spatial distribution statistical analysis. Landslides, 11(3), 441-461. https://doi.org/10.1007/s10346-013-0404-6

Yin, J.H., Chen, J., Xu, X.W., Wang, X.L. & Zheng, Y.G. (2010). The characteristics of the landslides triggered by the Wenchuan Ms 8.0 earthquake from Anxian to Beichuan. Journal of Asian Earth Sciences, 37(5-6), 452-459. https://doi.org/10.1016/j.jseaes.2009.12.002

Yin, Y.P., Wang, F.W. & Sun, P. (2009). Landslide hazards triggered by the 2008 Wenchuan earthquake, Sichuan, China. Landslides, 6(2), 139-151. https://doi.org/10.1007/s10346-009-0148-5

Yin, Z.Q., Qin, X.G., Wu, J.S. & Ning, B. (2009). The Multimodal Grain-Size Distribution Characteristics of Loess, Desert, Lake and River Sediments in Some Areas of Northern China. Acte Sedimentologica Sinica, 27(2), 343-351(in Chinese).

Zhang, F., Jin, Z.D., West, A.J., An, Z.S., Hilton, R.G., Wang, J., Li, G., Densmore, A.L., Yu, J.M., Qiang, X.K., Sun, Y.B., Li, L.B., Gou, L.F., Xu, Y., Xu, X.W., Liu, X.X., Pan, Y.H. & You, C.F. (2019). Monsoonal control on a delayed response of sedimentation to the 2008 Wenchuan earthquake. Science Advances, 5(6), eaav7110. https://doi.org/10.1126/sciadv.aav7110

Zhang, P., Zhou, Z.Y., Xu, C.H. & Zhang, Q.L. (2008). Geochemistry of Pengguan complex in the Longmenshan region, western Sichuan Province, SW China: petrogenesis and tectonic implications. Geotectonica et Metallogenia, 32(1), 105-116 (in Chinese).

Zhang, P.Z., Deng, Q.D., Zhang, M.G., Ma, J., Gan, W.J., Wei, M., Mao, F.Y. & Wang, Q. (2003). Active tectonic blocks and strong earthquakes in the continent of China. Science in China, 46(Supp.), 13-24. https://doi.org/10.1360/03dz0002

Zhang, X.S., Sun, S.Z., Yong, S.P., Zhuo, Z.D. & Wang, R.Q. (2007). Vegetation Map of China and its Geographic Pattern-illustration of the Vegetation Map of the People's Republic of China (1:1 000 000). Beijing, Geological Press (in Chinese).

Zhang, Y.Q., Yang, N. & Meng, H. (2005). Deep-incised valleys along the Minjiang river upstream and their responses to the uplift of the West Sichuan Plateau, China. Journal of Chengdu University Technology, 32(4), 331-339(in Chinese).

Zhou R.J., Li, Y., Densmore, A.L., Ellis, M.A., He, Y.L., Wang, F.L. & Li, X.G. (2006). Active tectonics of the eastern margin of the Tibet Plateau. Journal of Mineralogy and Petrology, 26(2),40-51(in Chinese).

Zhou, R.J., Pu, X.H., He, Y.L., Li, X.G. & Ge, T.Y. (2000). Recent activity of Minjiang fault zone, uplift of Minshan Block and their relationship with seismicity of Sichuan. Seismology and Geology, 22(3),285-294(in Chinese).

Zhong, N., Jiang, H.C., Li, H.B., Xu, H.Y., Shi, W., Zhang, S.Q. & Wei, X.T. (2019). Last Deglacial Soft-Sediment Deformation at Shawan on the Eastern Tibetan Plateau and Implications for Deformation Processes and Seismic Magnitudes. Acta Geologica Sinica, 93(2), 430-450. https://doi.org/10.1111/1755-6724.13773

Zondervan, J., Stokes, M., Boulton, S., Telfer, M. & Mather, A. (2020). Rock strength and structural controls on fluvial erodibility: Implications for drainage divide mobility in a collisional mountain belt. Earth and Planetary Science Letters 538, 116221. https://doi.org/10.1016/j.epsl.2020.116221

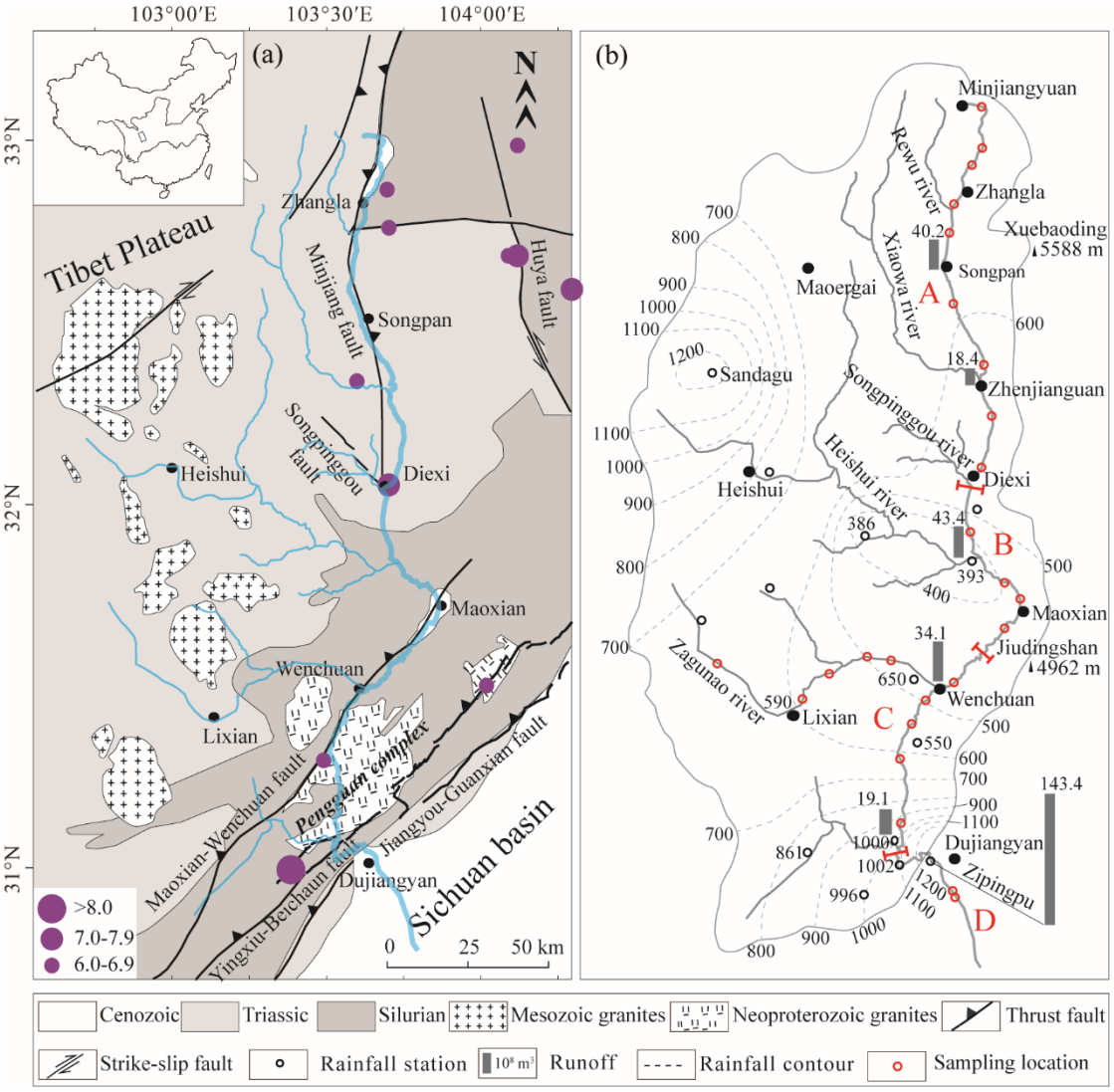

Figure 1. (a) Geological map and (b) precipitation distribution (Ding et al., 2014) of the upper Min River basin. Seismic data are from the China Earthquake Data Center (http://data.earthquake.cn/data).

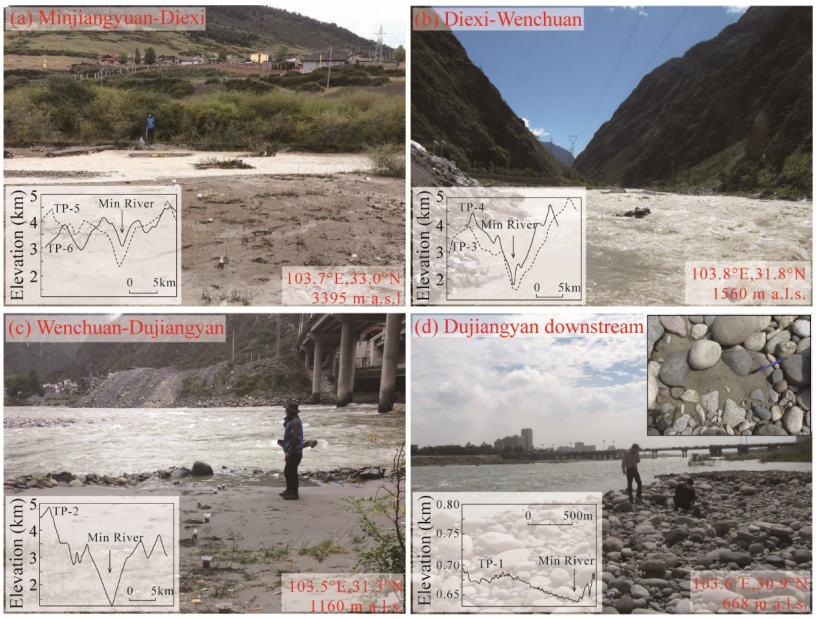

Figure 2. Field sampling photograph from the upper Min River. Cross-section positions of the Min River valleys (Zhang et al., 2005) are shown in Figure 7c.

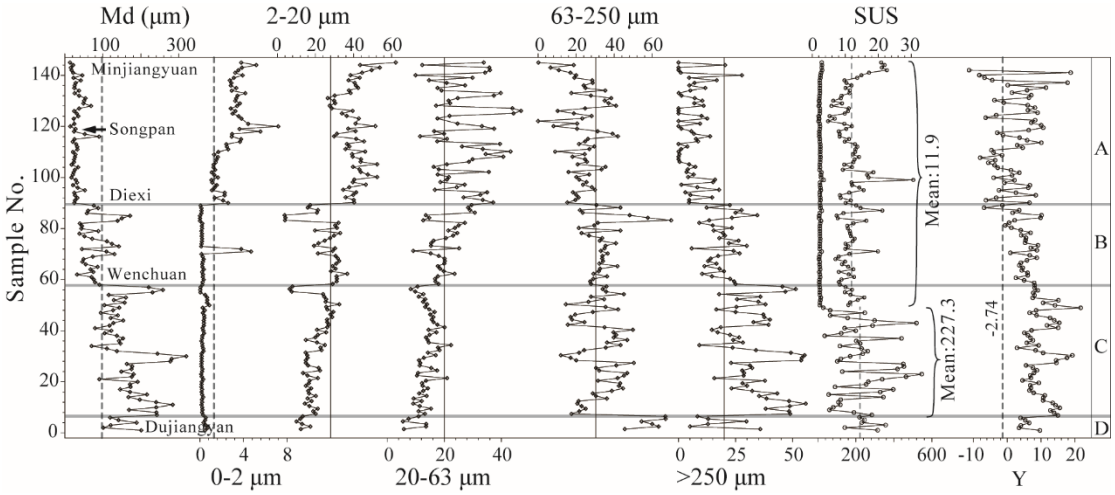

Figure 3. Variation of grain-size components and parameters of river sediments

from the upper Min River.

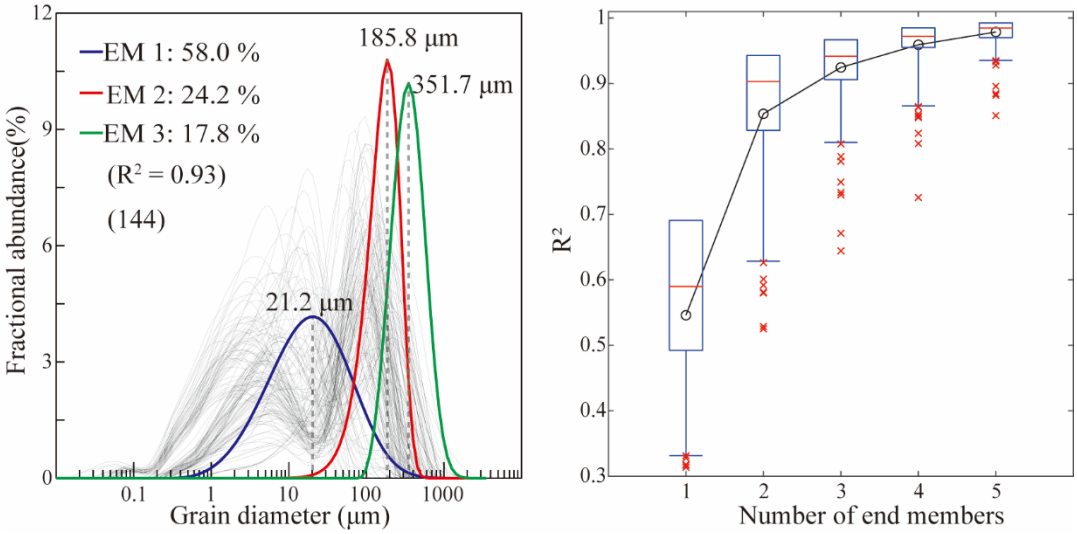

Figure 4. End-member analysis model of fluvial sediments from the upper Min River.

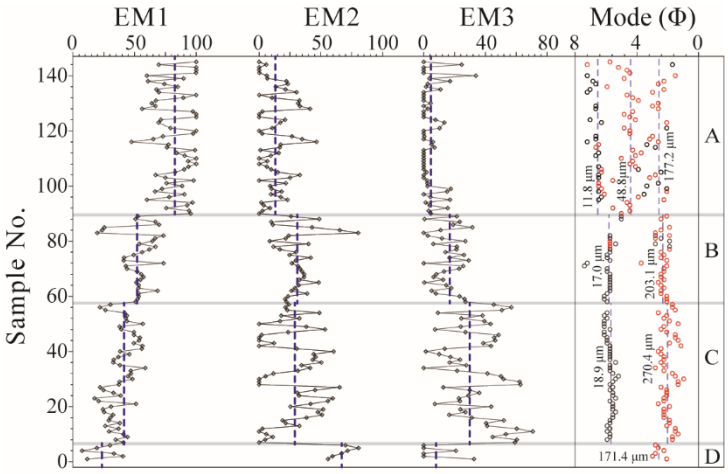

Figure 5. variability of the three EMs and the mode values from the upper Min River. Considering the 1% instrumental error, the fractional abundance >1% of the mode in a grain-size frequency distribution is extracted. The red and black circles represent the main and secondary peak mode values, respectively.

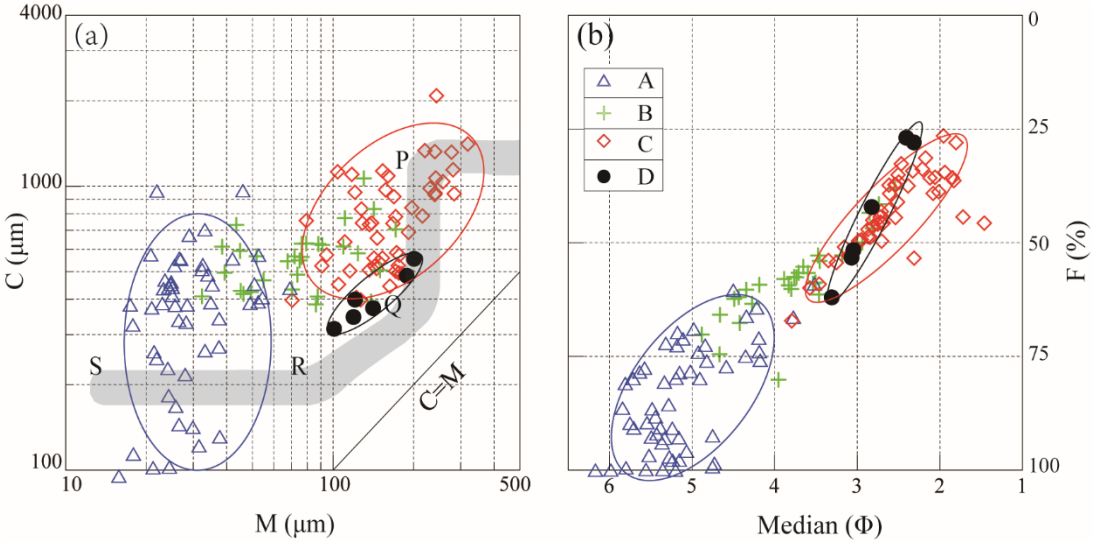

Figure 6. C-M and F-M distributions of the samples from the four segments of the upper Min River.

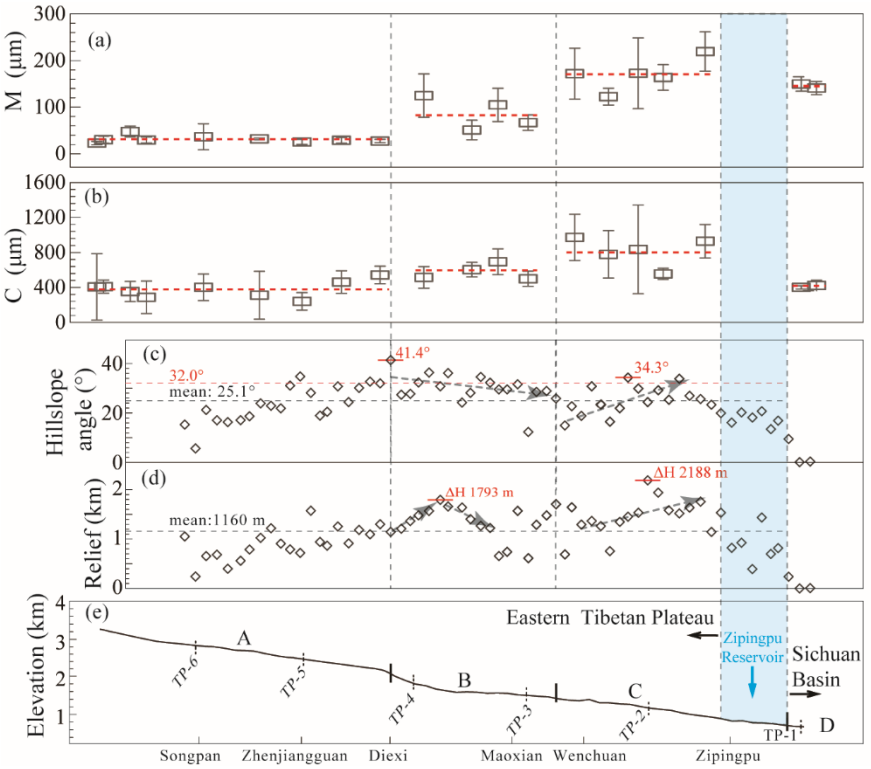

Figure 7. The variation characteristics of (a) M and (b) C values of the grain-

size index. (c) The riverbed base-level and the position of the cross-section of the upper Min River (Zhang et al., 2005). (d) Hillslope angle and (e) local relief along the upper Min River. A 4*4 km grid was delineated along the upper Min River (~260 km). The highest ridgeline and riverbed height in the grid were extracted from a DEM map, and then the local relief was obtained by calculating the highest ridgeline minus the riverbed height. The hillslope angle is obtained by tan (local relief/slope length).